

# Nanoscale

Accepted Manuscript

This article can be cited before page numbers have been issued, to do this please use: K. Takemae, S. Tomihari, T. Naitou, M. Takagi, T. Shimazaki, T. Kawawaki, M. Tachikawa and Y. Negishi, *Nanoscale*, 2025, DOI: 10.1039/D4NR04579C.



This is an Accepted Manuscript, which has been through the Royal Society of Chemistry peer review process and has been accepted for publication.

Accepted Manuscripts are published online shortly after acceptance, before technical editing, formatting and proof reading. Using this free service, authors can make their results available to the community, in citable form, before we publish the edited article. We will replace this Accepted Manuscript with the edited and formatted Advance Article as soon as it is available.

You can find more information about Accepted Manuscripts in the [Information for Authors](#).

Please note that technical editing may introduce minor changes to the text and/or graphics, which may alter content. The journal's standard [Terms & Conditions](#) and the [Ethical guidelines](#) still apply. In no event shall the Royal Society of Chemistry be held responsible for any errors or omissions in this Accepted Manuscript or any consequences arising from the use of any information it contains.

## ARTICLE

## Inclusion of Gold Ion in Tiara-Like Nickel Hexanuclear Nanoclusters

Kana Takemae,<sup>a,†</sup> Shiho Tomihari,<sup>a,†</sup> Takumi Naito,<sup>b</sup> Makito Takagi,<sup>b</sup> Tomomi Shimazaki,<sup>b</sup> Tokuhiwa Kawawaki,<sup>\*a,c</sup> Masanori Tachikawa<sup>\*b</sup> and Yuichi Negishi<sup>\*c,d</sup>Received 00th January 20xx,  
Accepted 00th January 20xx

DOI: 10.1039/x0xx00000x

Tiara-like metal nanoclusters (TNCs) composed of group 10 transition metals and thiolates can easily change their number of polymerization and include various molecules or metal ions as guests within their ring structures. Therefore, they are expected to be applied in sensing, storage, and catalyst materials based on the selective inclusion characteristics. However, there are very few reports regarding the principles of selective inclusion for guest molecules/ions in TNCs. In this study, we focused on the nickel (Ni) hexanuclear TNC, Ni<sub>6</sub>(PET)<sub>12</sub> (PET = 2-phenylethanethiolate), to clarify the kinds of the metal ions that can be included in TNCs. As a result, we found that gold (Au) ion can be selectively included in Ni<sub>6</sub>(PET)<sub>12</sub> among various metal ions to form a stable structure. From the various experiments and density functional theory calculations, we concluded that the main reasons for this are that [Ni<sub>6</sub>(PET)<sub>12</sub>]<sup>0</sup> has (1) a pore large enough to include Au ion and (2) Ni and Au favour the formation of bonding orbitals based on charge transfer interactions. These insights are expected to lead to a better understanding of host-guest interactions in TNCs and provide clear design guidelines for forming various inclusion structures in the future.

## Introduction

Multinuclear metal complexes, called metal nanoclusters (NCs), exhibit different physicochemical properties from those of bulk metals composed of the same metal elements.<sup>1, 2</sup> These metal NCs can be precisely synthesized as stable compounds using thiolate (SR) ligands.<sup>3-15</sup> Furthermore, the obtained metal NCs are attracting much attention as highly functional materials in fields such as catalysis,<sup>1, 16-21</sup> bio-imaging,<sup>22-25</sup> sensing,<sup>22, 23</sup> and optics<sup>26, 27</sup>. In particular, tiara-like metal NCs (TNCs), which are ring compounds containing metal ions, are known to exhibit high complexation ability with other metal ions and small organic molecules. Among them, [M(SR)<sub>2</sub>]<sub>n</sub> (M = Ni, Pd, Pt) composed of group 10 transition metals and SR can easily change its degree of polymerization, thus TNCs with different numbers of atoms can be size-selectively obtained.<sup>28-37</sup> In addition, [M(SR)<sub>2</sub>]<sub>n</sub> is more stable than other cyclic molecules such as crown ethers, cryptands, and cyclic dextrans because it has a relatively simple structure.

These TNCs have been reported to exhibit inclusion properties, trapping a guest molecule in the ring as a host molecule.<sup>30, 31, 38-41</sup> The inclusion properties of [M(SR)<sub>2</sub>]<sub>n</sub> (n = 8–12) have been reported, but

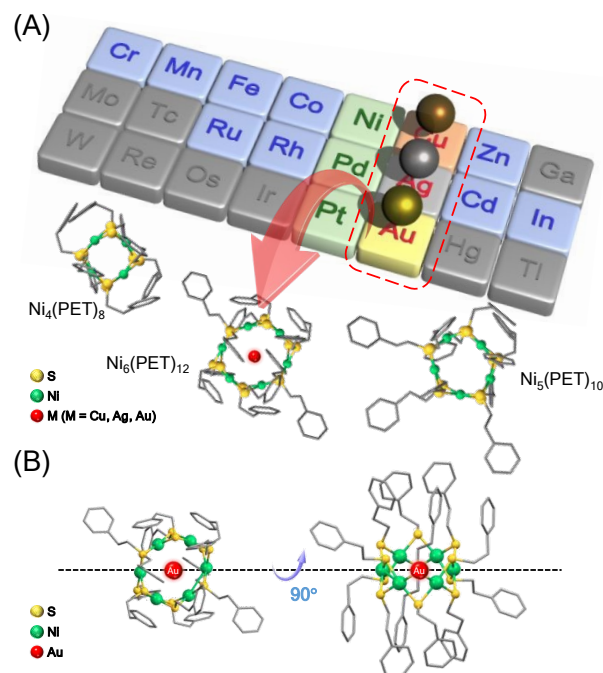


**Fig. 1** Schematic illustration of (A) the purposes of this study and (B) presumed geometric structure of gold ion-included Ni<sub>6</sub>(PET)<sub>12</sub>. In (B), the geometric structure of Ni<sub>6</sub>(PET)<sub>12</sub> after inclusion of transition metal ion is shown from several points of view.

<sup>a</sup> Department of Applied Chemistry, Faculty of Science, Tokyo University of Science, 1-3 Kagurazaka, Shinjuku-ku, Tokyo 162-8601, Japan

<sup>b</sup> Quantum Chemistry Division, Yokohama City University, 22-2 Seto, Kanazawa-ku, Yokohama, 236-0027, Japan

<sup>c</sup> Research Institute for Science and Technology, Tokyo University of Science, 1-3 Kagurazaka, Shinjuku-ku, Tokyo 162-8601, Japan

<sup>d</sup> Institute of Multidisciplinary Research for Advanced Materials, Tohoku University, 2-1-1 Katahira, Aoba-ku, Sendai 980-8577, Japan

<sup>†</sup> Supplementary Information available: [details of any supplementary information available should be included here]. See DOI: 10.1039/x0xx00000x

the guest molecules were limited to iodine molecules and solvent molecules.<sup>30,31,38,39</sup> Recently, it has been reported that a Pt hexanuclear TNC (Pt<sub>6</sub>(SR)<sub>12</sub>; SR = octanethiolate (C8) or



dodecanethiolate (C12)) selectively included a monovalent Ag ion ( $\text{Ag}^+$ ) and exhibits excellent phosphorescent properties.<sup>40, 41</sup> However, much is still unknown about what kinds of TNCs can include metal ions and their selectivity for metal ions. In particular, Ni TNCs ( $\text{Ni}_n(\text{SR})_{2n}$ ) have attracted much attention in recent years because of their host–guest chemistry, catalytic activity in the reduction of 4-nitrophenol, and hydrogen and oxygen production from water.<sup>30, 31, 42–46</sup> Therefore, when alloying by inclusion of different metal ions is achieved in Ni hexanuclear TNCs ( $\text{Ni}_6(\text{SR})_{12}$ ) with pores of the almost same size as  $\text{Pt}_6(\text{SR})_{12}$ ,<sup>28, 42–47</sup> it will lead to further functionalization of the TNCs. In this study, we attempted to synthesize metal ion-included  $\text{Ni}_6(\text{PET})_{12}$  (PET = 2-phenylethanethiolate) for these reasons. In addition, we investigated the selective inclusion of metal ions in a series of SR-protected metal hexanuclear TNCs ( $\text{M}_6(\text{SR})_{12}$ , M = Ni, Pd, Pt) to elucidate the host–guest interactions of  $[\text{M}(\text{SR})_2]_n$  (Fig. 1).

## Experimental

The precursor TNCs,  $[\text{Ni}_n(\text{PET})_{2n}]^0$  ( $n = 4, 5, 6$ ), were synthesized following previously reported methods,<sup>21</sup> and the crude products were separated using thin-layer chromatography (TLC; Fig. S1). The purity of the obtained  $[\text{Ni}_6(\text{PET})_{12}]^0$  was confirmed using ultraviolet-visible absorption spectroscopy, matrix-assisted laser desorption/ionization-mass spectrometry (MALDI-MS), Fourier transform infrared spectroscopy, and X-ray absorption fine structure analysis (Fig. 2, S2, and S3).

### Screening for metal ion inclusion in $\text{Ni}_6(\text{PET})_{12}$

Metal ion-included  $\text{Ni}_6(\text{PET})_{12}$  was synthesized using the method for synthesizing  $\text{Ag}^+$ -included  $\text{Pt}_6(\text{SR})_{12}$  ( $\text{AgPt}_6(\text{SR})_{12}$ ; SR = C8 or C12) reported by Konishi *et al.*<sup>40</sup> and Yamamoto *et al.*<sup>41</sup> with slight modification (Fig. S4). An acetonitrile solution (2 mL) containing each metal ion precursors (Cr, Mn, Fe, Co, Cu, Zn, Ru, Rh, Ag, Cd, In, or Au ions; 1.0 equiv.) was added to a toluene solution (10 mL) containing  $\text{Ni}_6(\text{PET})_{12}$  (1.998 mg, 1  $\mu\text{mol}$ ) and the resulting solution was stirred for 10 min. The reaction solvent was then removed using a rotary evaporator, and the obtained product was extracted with dichloromethane (DCM). Metal ion-included  $\text{Ni}_6(\text{PET})_{12}$  was obtained by filtration through a Minisart® to remove the insoluble part. The obtained product was evaluated to screen for the metal ion-included  $\text{Ni}_6(\text{PET})_{12}$ .

### Synthesis method for $\text{MNi}_6(\text{PET})_{12}$ (M = Cu, Ag, Au)

Tetrahydrofuran (THF) was selected as the reaction solvent due to the high solubility of both the  $[\text{Ni}_6(\text{PET})_{12}]^0$  and metal salts ( $\text{CuCl}_2$ ,  $\text{AgCl}$ , and  $\text{HAuCl}_4$ ) in THF.  $[\text{Ni}_6(\text{PET})_{12}]^0$  (1.998 mg, 1  $\mu\text{mol}$ ) was dissolved in THF (10 mL), followed by the addition of a THF solution (2 mL) of the metal salts (1  $\mu\text{mol}$ ). The mixture was stirred at 60 °C for 30 min. After the reaction, the solvent was removed using a rotary evaporator. The resulting crude product was extracted with DCM, followed by filtration through a Minisart® to remove the insoluble part. The crude product was further purified using TLC (DCM:hexane = 3:4, v/v). The first band from the top of the TLC plate was collected (Fig. S5) and extracted with DCM to yield  $[\text{MNi}_6(\text{PET})_{12}]^+$  (Fig. S6).

## Results and discussion

### Metal ion inclusion in $\text{Ni}_6(\text{PET})_{12}$

Transition metal ions from group 6 to 13 (Cr, Mn, Fe, Co, Cu, Zn, Ru, Rh, Ag, Cd, In, and Au) were utilized to investigate the metal ion inclusion in the typical Ni TNC,  $[\text{Ni}_6(\text{PET})_{12}]^0$ . Each metal ion was added to  $[\text{Ni}_6(\text{PET})_{12}]^0$ , and changes in the optical absorption spectra and MALDI–MS spectra of the resulting products were examined. As a result, for many kinds of metal ions, the products obtained upon the addition of metal ions exhibited no significant change in spectral shape compared with  $[\text{Ni}_6(\text{PET})_{12}]^0$ , whereas significant changes occurred when Cu, Ag, and Au ions were added (Fig. 2 and S7).

The MALDI–MS spectra of  $[\text{Ni}_6(\text{PET})_{12}]^0$  and the product (**1**) obtained after the addition of  $\text{HAuCl}_4$  and subsequent purification are presented in Fig. 2A (Table S1). In the MS spectrum of **1**, a peak was detected at a mass-to-charge ratio ( $m/z$ ) of 2195, which differed from that of  $[\text{Ni}_6(\text{PET})_{12}]^0$ . Upon comparing the isotope pattern of **1** with that of the simulated Au ion-included  $\text{Ni}_6(\text{PET})_{12}$  ( $[\text{AuNi}_6(\text{PET})_{12}]^+$ ) (Fig. 2A inset), it was found that **1** primarily contains  $[\text{AuNi}_6(\text{PET})_{12}]^+$  as the main product. In addition, as byproducts, the existence of  $[\text{AuNi}_7(\text{PET})_{14}]^+$  and  $[\text{AuNi}_8(\text{PET})_{16}]^+$ , in which Au ion is doped into larger Ni TNCs ( $\text{Ni}_7(\text{PET})_{14}$  and  $\text{Ni}_8(\text{PET})_{16}$ ), and  $[\text{Au}_2\text{Ni}_3(\text{PET})_8]^+$ , a double-crown structure alloy TNC,<sup>48</sup> were also observed with small amounts. These results indicate that

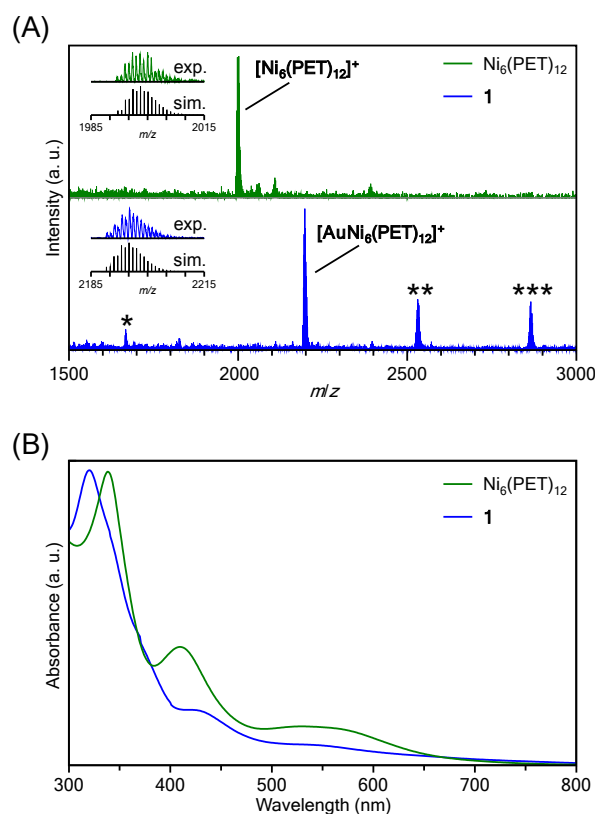


**Fig. 2** (A) Positive-ion MALDI-MS spectra before and after Au ion inclusion into  $[\text{Ni}_6(\text{PET})_{12}]^0$ . Insets show a comparison of the isotope patterns between the experimental spectrum and calculated one. The peaks with “\*”, “\*\*”, and “\*\*\*” were assigned to  $[\text{Au}_2\text{Ni}_3(\text{PET})_8]^+$ ,  $[\text{AuNi}_7(\text{PET})_{14}]^+$ , and  $[\text{AuNi}_8(\text{PET})_{16}]^+$ , respectively. (B) Optical absorption spectra before and after Au ion inclusion into  $[\text{Ni}_6(\text{PET})_{12}]^0$ .



$[\text{Ni}_6(\text{PET})_{12}]^0$  has a relatively flexible structure in solution, allowing for the dissociation and polymerization of  $\text{Ni}(\text{PET})_2$  units during the reaction. The formation of  $[\text{AuNi}_6(\text{PET})_{12}]^+$  was also confirmed when a Au(I) was used as a precursor (Fig. S7B). Unfortunately, it was difficult to isolate  $[\text{AuNi}_6(\text{PET})_{12}]^+$  with high purity for these reasons, and thereby obtain a single crystal of  $[\text{AuNi}_6(\text{PET})_{12}]^+$ .

The existence of Au and Ni in **1** was also confirmed using inductively coupled plasma-MS. The optical absorption spectrum of  $[\text{Ni}_6(\text{PET})_{12}]^0$  exhibited absorption peaks at around 340 nm and 410 nm (Fig. 2B), but for **1**, peaks were observed at around 320 nm and 430 nm, and the shape of the absorption spectrum had changed from that of  $[\text{Ni}_6(\text{PET})_{12}]^0$  (Fig. 2B). We further examined the electronic states of  $[\text{Ni}_6(\text{PET})_{12}]^0$  and **1** using X-ray photoelectron spectroscopy (Fig. S8). As a result, the peak of the Ni 2p spectrum was shifted to a slightly higher energy region in the spectrum of **1** than that of  $[\text{Ni}_6(\text{PET})_{12}]^0$ , indicating that the charge state of Ni became a slightly positive by the inclusion of Au ion into  $[\text{Ni}_6(\text{PET})_{12}]^0$ . In addition, it was found that the electronic state of the included Au was relatively close to that of a metal (Fig. S8). Density functional theory (DFT) calculations conducted on Ag ion-included  $\text{Pt}_6(\text{SR})_{12}$  ( $[\text{AgPt}_6(\text{SR})_{12}]^+$ ), also have reported a similar tendency: the electronic state of the included Ag ion was relatively close to that of a metal.<sup>40</sup> These results indicate that the included Au ion coordinates to the  $\text{Ni}_6(\text{PET})_{12}$  structure while receiving a partial electron from Ni or S. Fig. S9A shows the time-dependent change in the optical absorption spectrum of **1** in THF solution at room temperature. The absorption spectrum did not change even after 24 h, indicating that **1** is a stable compound like  $[\text{Ni}_6(\text{PET})_{12}]^0$  (Fig. S9B). Due to this change in electronic structure, **1** exhibited superior activity for the hydrogen evolution reaction compared to  $\text{Ni}_6(\text{PET})_{12}$  (Fig. S10). The doping

properties of other group 11 metal ions (Cu, Ag and Au) in  $[\text{Ni}_6(\text{PET})_{12}]^0$  were also investigated. Fig. S7 shows the MALDI-MS spectrum of the products obtained by adding  $\text{CuCl}_2$  to  $[\text{Ni}_6(\text{PET})_{12}]^0$ . The peak intensity at  $m/z = 1998$  derived from  $\text{Ni}_6(\text{PET})_{12}$  decreases and a new peak attributed to Cu ion-doped  $\text{Ni}_6(\text{PET})_{12}$  ( $[\text{CuNi}_6(\text{PET})_{12}]^+$ ) appeared at  $m/z = 2061$  (Table S2) by the addition of  $\text{CuCl}_2$ . When  $\text{AgCl}$  was added to  $[\text{Ni}_6(\text{PET})_{12}]^0$ , the peak intensity of  $\text{Ni}_6(\text{PET})_{12}$  decreased, and a new peak was detected at  $m/z = 2105$  that was attributed to Ag ion-doped  $\text{Ni}_6(\text{PET})_{12}$  ( $[\text{AgNi}_6(\text{PET})_{12}]^+$ ; Fig. S7 and Table S2). From these results, it can be considered that Cu and Ag ions can also be included in  $[\text{Ni}_6(\text{PET})_{12}]^0$ . However, it was difficult to stably extract these products in high purity.

Thus, it was found that  $[\text{Ni}_6(\text{PET})_{12}]^0$  selectively includes Au, Ag, and Cu ions among the major metals from group 6 to 13, and the resulting  $\text{AuNi}_6(\text{PET})_{12}$  exhibits higher stability than  $\text{AgNi}_6(\text{PET})_{12}$  and  $\text{CuNi}_6(\text{PET})_{12}$ .

### Electronic/geometric structure of $[\text{AuNi}_6(\text{PET})_{12}]^+$

We performed DFT calculations on  $[\text{Ni}_6(\text{PET})_{12}]^0$  and  $[\text{AuNi}_6(\text{PET})_{12}]^+$  to elucidate the reason why Au ion can be stably included within  $[\text{Ni}_6(\text{PET})_{12}]^0$ . Fig. 3 shows the geometrical structure of  $[\text{AuNi}_6(\text{PET})_{12}]^+$  obtained through structural optimization using DFT calculations. From the normal vibration analysis, it was found that  $[\text{AuNi}_6(\text{PET})_{12}]^+$  has thermodynamically stable compared with  $[\text{Ni}_6(\text{PET})_{12}]^0$ . Similar calculations were also performed for  $[\text{Ni}_6(\text{PET})_{12}]^0$  and  $[\text{AuNi}_6(\text{PET})_{12}]^+$  in THF, the actual reaction solvent. The results implied that the inclusion of  $\text{Au}^+$  into  $[\text{Ni}_6(\text{PET})_{12}]^0$ ,  $[\text{AuNi}_6(\text{PET})_{12}]^+$  causes the thermodynamical stability of 63.0 kcal/mol, compared with  $\text{Au}^+ + [\text{Ni}_6(\text{PET})_{12}]^0$ . We also performed DFT calculations on Ag and Cu with ion-included  $\text{Ni}_6(\text{PET})_{12}$  in THF (Table. S3). Those calculations show that  $\text{Ag}^+$  and  $\text{Cu}^+$  are more stabilized by the inclusion into  $\text{Ni}_6(\text{PET})_{12}$  (31.1 and 44.8 kcal/mol for  $[\text{AgNi}_6(\text{PET})_{12}]^+$  and  $[\text{CuNi}_6(\text{PET})_{12}]^+$ , respectively). Thus, we confirmed that Au is most stabilized. From the Mulliken charge analysis,  $\text{Ag}^+$  and  $\text{Cu}^+$  tend to remain cationic, but  $\text{Au}^+$  is close to neutral due to the large charge transfer, suggesting that stronger interaction between Au and the  $\text{Ni}_6(\text{PET})_{12}$ . These calculations are consistent with the experimental results.

This stabilization is likely due to the hybridization of the orbitals between the Au ion and the Ni and S in the ring structure. Accordingly, we calculated the electronic structures and optical absorption spectra of  $[\text{Ni}_6(\text{PET})_{12}]^0$  and  $[\text{AuNi}_6(\text{PET})_{12}]^+$  with the optimized structures. The calculated absorption spectrum of  $[\text{Ni}_6(\text{PET})_{12}]^0$  showed several peaks corresponding to charge transfer (CT) transitions between the orbitals mainly consisting of S and Ni atoms (Fig. S11). The peak at around 340 nm is mainly attributed to ligand-to-metal CT (LMCT) transitions, and the peak at around 410 nm is mainly attributed to Ni d–d transitions. On the other hand, in the calculated absorption spectrum of  $[\text{AuNi}_6(\text{PET})_{12}]^+$  (Fig. 4), the peak due to d–d transitions specifically localized to Ni and Au were observed at around 340 nm. It was found that specific localization to Au also occurs in the LMCT transition at 420 nm. A new absorption band was also observed at approximately 660 nm, which is mainly attributed to the transition from the orbitals of Ph group to those of Au 6s (Fig. 4). These new hybrid orbitals caused by the inclusion of Au ion into  $[\text{Ni}_6(\text{PET})_{12}]^0$  is considered to influence the interaction between the Ni and S atoms in the original  $[\text{Ni}_6(\text{PET})_{12}]^0$ , and thereby

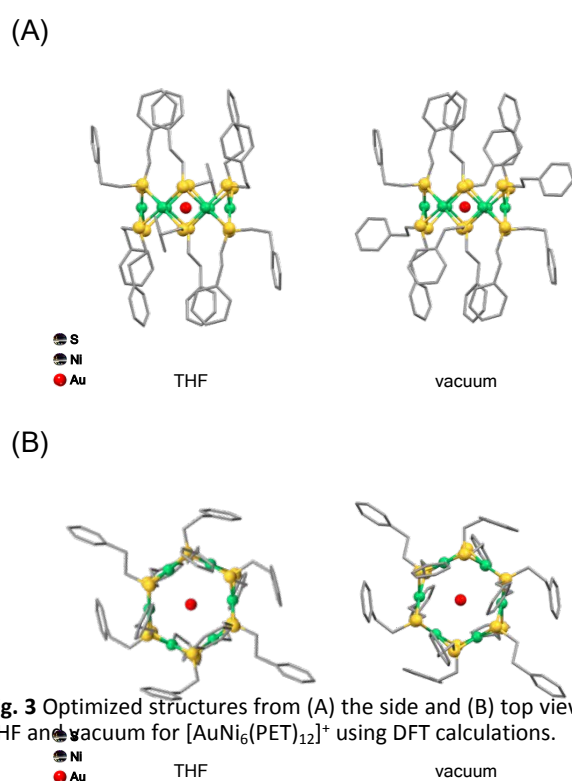


**Fig. 3** Optimized structures from (A) the side and (B) top view in THF and vacuum for  $[\text{AuNi}_6(\text{PET})_{12}]^+$  using DFT calculations.





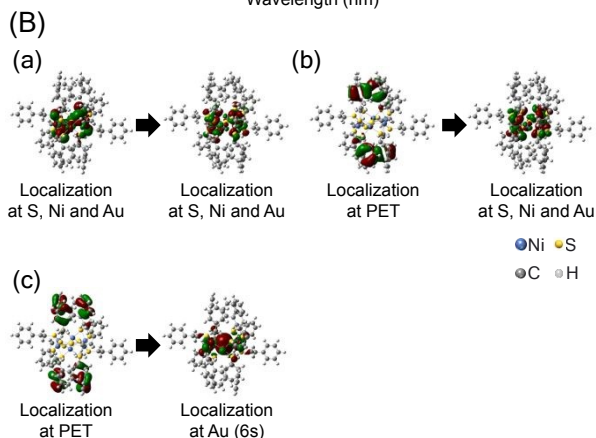
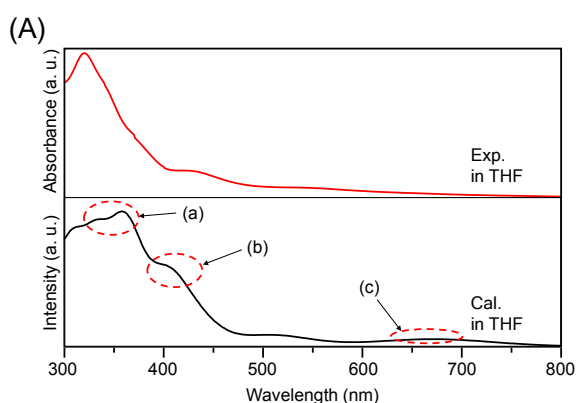


**Fig. 4** (A) Experimental (red) and calculated (black) absorption spectra for  $[\text{AuNi}_6(\text{PET})_{12}]^+$  in THF. (B) (a)–(c) Molecular orbitals of  $[\text{AuNi}_6(\text{PET})_{12}]^+$  for main peaks observed in the calculated spectrum in THF at (a)–(c) in (A).

cause slight changes in the energy of each orbital. Indeed, the previous studies<sup>39–41</sup> reported that when  $[\text{M}(\text{SR})_2]_n$  includes solvent molecules or metal ions, the changes occur in the M–S bond distance to maintain their structure. Therefore, it can be considered that the overall structural changes in the absorption spectrum due to the inclusion of Au ion are also caused by the change in the bonding properties of the TNC framework. In fact, the Ni–S and Ni–Ni bond distances of  $[\text{AuNi}_6(\text{PET})_{12}]^+$  in THF, which were estimated by DFT calculations, were shorter than those of  $[\text{Ni}_6(\text{PET})_{12}]^0$ , and the TNC structure shrank overall due to the inclusion (Table S4). Furthermore, we performed the natural bond order analysis (Table S3). We found that the bond order of Au–Ni is relatively high, while that of Au–S is small for  $[\text{AuNi}_6(\text{PET})_{12}]^+$ . Small bond orders on S are similarly observed for other metal ion from the calculations for  $[\text{AgNi}_6(\text{PET})_{12}]^+$  and  $[\text{CuNi}_6(\text{PET})_{12}]^+$ . This suggests that the interaction with Ni sites of  $\text{Ni}_6(\text{PET})_{12}$  plays essential roles on the metal inclusion. From these results, we can consider that for  $[\text{Ni}_6(\text{PET})_{12}]^0$ , Au ion is suitable for orbital hybridization and inducing stabilization without distorting the TNC structure. Considering the fact that a similar interpretation has also obtained for  $[\text{AgPt}_6(\text{C12})_{12}]^+$ ,<sup>40</sup> it can be concluded that in the formation of metal ion-included TNCs composed of group 10 elements as hosts, the main driving force for inclusion is whether the guest group 11 elements can easily form the bonding orbitals with host TNCs.

#### Metal ion inclusion in $\text{M}_6(\text{PET})_{12}$ (M = Ni, Pd, Pt)

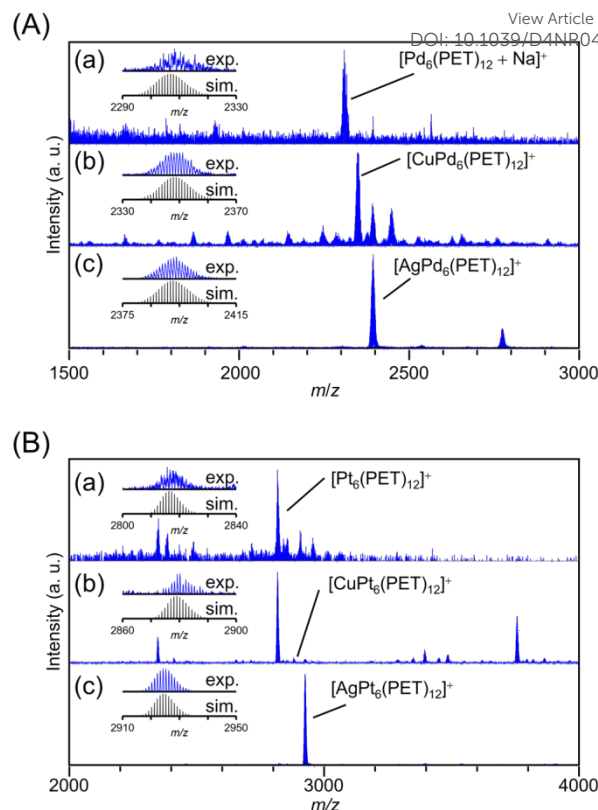


**Fig. 5** Positive-ion MALDI mass spectra (a) before and after adding (b) Cu(I) and (c) Ag(I) salts into (A)  $\text{Pd}_6(\text{PET})_{12}$  and (B)  $\text{Pt}_6(\text{PET})_{12}$  solutions. Insets show the comparison of the isotope patterns between the experimental spectrum (blue) and calculated one (black). Several peaks attributed to byproducts were assigned and summarized in Tables S5 and S6.

We also investigated whether the hexanuclear TNCs  $[\text{M}_6(\text{PET})_{12}]^0$  (M = Ni, Pd, Pt) can include metal ions as well (Fig. 5, Tables S5 and S6). The MALDI–MS spectra suggested that for Pt TNC ( $[\text{Pt}_6(\text{PET})_{12}]^0$ ) and Pd TNC ( $[\text{Pd}_6(\text{PET})_{12}]^0$ ), Cu and Ag ions were selectively included, whereas Au ion was not included (Fig. 5). This result is consistent with the previous studies,<sup>40,41</sup> in which Ag ion was included in  $[\text{Pt}_6(\text{SR})_{12}]^0$  (SR = C8 or C12), indicating that difference in the kinds of SR ligand (PET vs. C8 vs. C12) affects only little on the selectivity of the included metal ion in  $[\text{M}_6(\text{SR})_{12}]^0$ .

To deepen our understanding on the origin of the selectivity of metal ions, we next investigated the correlation between the ring spaces and the size of the included metal ions. The diagonal metal-to-metal distances are 6.34, 6.24, and 5.85 Å for  $[\text{Pt}_6(\text{SR})_{12}]^0$ ,  $[\text{Pd}_6(\text{SR})_{12}]^0$ , and  $[\text{Ni}_6(\text{SR})_{12}]^0$ , respectively.<sup>33,40,49</sup> From these values and the van der Waals radii<sup>49</sup> of each metal ion, the pore sizes of  $[\text{Pt}_6(\text{SR})_{12}]^0$ ,  $[\text{Pd}_6(\text{SR})_{12}]^0$ , and  $[\text{Ni}_6(\text{SR})_{12}]^0$  have been estimated to be 2.84,<sup>40</sup> 2.98,<sup>33</sup> and 2.59 Å,<sup>21</sup> respectively. Here, the ionic diameters of  $\text{Cu}^+$ ,  $\text{Ag}^+$ , and  $\text{Au}^+$  ions are 1.92, 2.52, and 2.74 Å, respectively.<sup>50</sup> These results indicate that even though the pore of  $[\text{Ni}_6(\text{SR})_{12}]^0$  is smaller than those of  $[\text{Pt}_6(\text{SR})_{12}]^0$  and  $[\text{Pd}_6(\text{SR})_{12}]^0$ , the larger size group 11 metal ions, Au ions, were included into  $[\text{Ni}_6(\text{PET})_{12}]^0$ . These results indicate that the match between the size of the pore and included metal ions is not sufficient to explain the selective inclusion of metal ions (Fig. S12). It can be assumed that the ease of inclusion changes depending on the binding energy between the Au ions and group 10



elements of the TNCs. In fact, the previous studies reported<sup>40,41</sup> that the six Pt–Ag bonds are not of equal length in  $[\text{AgPt}_6(\text{SR})_{12}]^+$ , but are biased, indicating that the relatively strong interaction (bonding) occurs between  $\text{Ag}^+$  and  $[\text{Pt}_6(\text{SR})_{12}]^0$ . Therefore, it can be presumed that the ease of constructing their bonding orbitals is the main driving force for the inclusion, rather than the match between the size of the TNCs pore and the metal ion to be included.

Finally, we show the result for the inclusion properties obtained using  $[\text{Ni}_4(\text{PET})_8]^0$  or  $[\text{Ni}_5(\text{PET})_{10}]^0$  as a precursor. In this case, only a small amount of  $\text{Ni}_4(\text{PET})_8$  or  $\text{Ni}_5(\text{PET})_{10}$  doped with group 11 elements was observed in the MALDI–MS spectra (Fig. S13–S15, Table S7). These results imply that the TNCs must have pores at least similar or larger than the size of the group 11 element ions to cause the inclusion. In addition, the introduction of Ag or Au ions resulted in peaks corresponding to  $[\text{AuNi}_n(\text{PET})_{2n}]^+$  ( $n = 6–8$ ) and  $[\text{AgNi}_6(\text{PET})_{12}]^+$  in the MALDI–MS spectra (Fig. S13–S15), despite using high-purity  $[\text{Ni}_4(\text{PET})_8]^0$  and  $[\text{Ni}_5(\text{PET})_{10}]^0$  as precursors. This result confirms the above assumption that the dissociation and polymerization of  $\text{Ni}(\text{SR})_2$  units in  $[\text{Ni}_n(\text{SR})_{2n}]^0$  occur relatively easily in solution, leading to the transformation into more thermodynamically stable TNC structures. For relatively small TNCs such as  $[\text{M}_4(\text{SR})_8]^0$  ( $\text{M} = \text{Ni}, \text{Pd}, \text{Pt}$ ) and  $[\text{Pd}_5(\text{SR})_{10}]^0$ , there are also a possibility that the doping with Au or Ag induces the formation of a double-crown shell structure.<sup>48,51–54</sup> Indeed, in our study, when heterometal ions were introduced into  $[\text{Ni}_4(\text{PET})_8]^0$ , weak peaks corresponding to the double-crown shell structure were observed.

Based on the above results, it can be concluded that the primary factors for forming stable metal ion-included TNCs composed of group 10 elements as hosts are: 1) the TNCs have pores similar or larger than the size of the included metal ions and 2) the formation of bonding orbitals between the included metal ions and the TNCs are promoted.

## Conclusions

In this study, we aimed to understand the selectivity of the inclusion of the metal ions within a ring structure of TNCs and the factors contributing to this process using SR-protected Ni, Pt, and Pd TNCs as hosts. As a result, we elucidated that  $[\text{Ni}_6(\text{PET})_{12}]^0$  selectively includes Cu, Ag, and Au ions, which are group 11 elements, in solution. Notably, the Au ion-included  $\text{Ni}_6(\text{PET})_{12}$  ( $[\text{AuNi}_6(\text{PET})_{12}]^+$ ) exhibited high stability. The various experimental and theoretical studies suggested that  $[\text{Ni}_6(\text{PET})_{12}]^0$  has: 1) pores of sufficient size that can include Au ions and 2) Ni ions that facilitate the formation of bonding orbitals with Au ions. Furthermore, investigation of the ease of inclusion for various ions ( $\text{Cu}^+$ ,  $\text{Ag}^+$  and  $\text{Au}^+$ ) into  $[\text{M}_6(\text{SR})_{12}]^0$  ( $\text{M} = \text{Ni}, \text{Pd}$  and  $\text{Pt}$ ) suggested that the main driving force for the inclusion was not the compatibility between the size of TNC pore and the metal ion, but the ease of constructing the bonding orbitals. These findings are expected to contribute to a better understanding of host–guest interactions in TNC systems and provide clear design guidelines for the formation of various inclusion complexes.

## Author contributions

T. Kawawaki and Y. Negishi designed the experiments and conducted the measurements with K. Takemae and S. Tomihara. T. Naito, M. Takagi, T. Shimazaki and M. Tachikawa performed the DFT calculations. T. Kawawaki, M. Tachikawa and Y. Negishi wrote the paper. All authors approved the final version of the manuscript.

## Conflicts of interest

There are no conflicts to declare.

## Data availability

Relevant data are available from the corresponding authors (T. Kawawaki, M. Tachikawa and Y. Negishi) upon reasonable request.

## Acknowledgements

The authors thank Mr. Tomoshige Okada, Sota Funaki and Yuki Iwamatsu (Tokyo University of Science) for their technical assistance. This work was supported by the Japan Society for the Promotion of Science (JSPS) KAKENHI (grant numbers 22K19012, 23H00289, and 24K01459). Funding from the Takahashi Industrial and Economic Research Foundation, the Carbon Recycling Fund Institute, the Japan Gas Association, the Iwatani Naoji Foundation, the Ichimura Foundation for New Technology, Suzuki Foundation, and Japan Keirin Autorace Foundation is also gratefully acknowledged.

## Notes and references

- 1 T. Kawawaki, A. Ebina, Y. Hosokawa, S. Ozaki, D. Suzuki, S. Hossain and Y. Negishi, *Small*, 2021, **17**, 2005328.
- 2 T. Kawawaki, Y. Imai, D. Suzuki, S. Kato, I. Kobayashi, T. Suzuki, R. Kaneko, S. Hossain and Y. Negishi, *Chem. -Eur. J.*, 2020, **26**, 16150–16193.
- 3 S. Takano, S. Hasegawa, M. Suyama and T. Tsukuda, *Acc. Chem. Res.*, 2018, **51**, 3074–3083.
- 4 R. L. Whetten, H.-C. Weissker, J. J. Pelayo, S. M. Mullins, X. López-Lozano and I. L. Garzón, *Acc. Chem. Res.*, 2019, **52**, 34–43.
- 5 I. Chakraborty and T. Pradeep, *Chem. Rev.*, 2017, **117**, 8208–8271.
- 6 Q. Yao, T. Chen, X. Yuan and J. Xie, *Acc. Chem. Res.*, 2018, **51**, 1338–1348.
- 7 Z. Gan, N. Xia and Z. Wu, *Acc. Chem. Res.*, 2018, **51**, 2774–2783.
- 8 Q. Tang, G. Hu, V. Fung and D.-e. Jiang, *Acc. Chem. Res.*, 2018, **51**, 2793–2802.
- 9 B. Nieto-Ortega and T. Bürgi, *Acc. Chem. Res.*, 2018, **51**, 2811–2819.
- 10 C. M. Aikens, *Acc. Chem. Res.*, 2018, **51**, 3065–3073.
- 11 B. Bhattarai, Y. Zaker, A. Atnagulov, B. Yoon, U. Landman and T. P. Bigioni, *Acc. Chem. Res.*, 2018, **51**, 3104–3113.
- 12 Y. Pei, P. Wang, Z. Ma and L. Xiong, *Acc. Chem. Res.*, 2019, **52**, 23–33.
- 13 C. A. Hosier and C. J. Ackerson, *J. Am. Chem. Soc.*, 2019, **141**, 309–314.
- 14 S. Chen, S. Wang, J. Zhong, Y. Song, J. Zhang, H. Sheng, Y. Pei and M. Zhu, *Angew. Chem., Int. Ed.*, **54**, 3145–3149.



- 15 W. Du, S. Jin, L. Xiong, M. Chen, J. Zhang, X. Zou, Y. Pei, S. Wang and M. Zhu, *J. Am. Chem. Soc.*, 2017, **139**, 1618–1624.
- 16 T. Kawawaki, Y. Kataoka, M. Hirata, Y. Iwamatsu, S. Hossain and Y. Negishi, *Nanoscale Horiz.*, 2021, **6**, 409–448.
- 17 T. Kawawaki, Y. Kataoka, S. Ozaki, M. Kawachi, M. Hirata and Y. Negishi, *Chem. Commun.*, 2021, **57**, 417–440.
- 18 T. Kawawaki, Y. Mori, K. Wakamatsu, S. Ozaki, M. Kawachi, S. Hossain and Y. Negishi, *J. Mater. Chem. A*, 2020, **8**, 16081–16113.
- 19 B. Kumar, T. Kawawaki, N. Shimizu, Y. Imai, D. Suzuki, S. Hossain, L. V. Nair and Y. Negishi, *Nanoscale*, 2020, **12**, 9969–9979.
- 20 C. Garcia, V. Truttman, I. Lopez, T. Haunold, C. Marini, C. Rameshan, E. Pittenauer, P. Kregsamer, K. Dobrezberger, M. Stöger-Pollach, N. Barrabés and G. Rupprechter, *J. Phys. Chem. C*, 2020, **124**, 23626–23636.
- 21 S. Funaki, T. Kawawaki, T. Okada, K. Takemae, S. Hossain, Y. Niihori, T. Naito, M. Takagi, T. Shimazaki, S. Kikkawa, S. Yamazoe, M. Tachikawa and Y. Negishi, *Nanoscale*, 2023, **15**, 5201–5208.
- 22 T. Kawawaki, Y. Negishi and H. Kawasaki, *Nanoscale Adv.*, 2020, **2**, 17–36.
- 23 M.-M. Zhang, K. Li and S.-Q. Zang, *Adv. Opt. Mater.*, 2020, **8**, 1902152.
- 24 X. Jiang, B. Du, Y. Huang and J. Zheng, *Nano Today*, 2018, **21**, 106–125.
- 25 F. Yu, Z. Cao, S. He, H. Xiang, G. Zhao, L. Yang and H. Liu, *Chem. Commun.*, 2022, **58**, 811–814.
- 26 X. Wang, B. Yin, L. Jiang, C. Yang, Y. Liu, G. Zou, S. Chen and M. Zhu *Science*, 2023, **381**, 784–790.
- 27 S. Wang, X. Meng, A. Das, T. Li, Y. Song, T. Cao, X. Zhu, M. Zhu and R. Jin, *Angew. Chem., Int. Ed.*, 2014, **53**, 2376–2380.
- 28 Y. Pan, J. Chen, S. Gong and Z. Wang, *Dalton Trans.*, 2018, **47**, 11097–11103.
- 29 C. Tan, M. Jin, X. Ma, Q. Zhu, Y. Huang, Y. Wang, S. Hu, T. Sheng and X. Wu, *Dalton Trans.*, 2012, **41**, 8472–8476.
- 30 S. A. Ivanov, M. A. Kozee, W. A. Merrill, S. Agarwal and L. F. Dahl, *J. Chem. Soc., Dalton Trans.*, 2002, 4105–4115.
- 31 C. Zhang, T. Matsumoto, M. Samoc, S. Petrie, S. Meng, T. C. Corkery, R. Stranger, J. Zhang, M. G. Humphrey and K. Tatsumi, *Angew. Chem., Int. Ed.*, 2010, **49**, 4209–4212.
- 32 T. Imaoka, Y. Akanuma, N. Haruta, S. Tsuchiya, K. Ishihara, T. Okayasu, W.-J. Chun, M. Takahashi and K. Yamamoto, *Nat. Commun.*, 2017, **8**, 688.
- 33 J. Chen, L. Liu, L. Weng, Y. Lin, L. Liao, C. Wang, J. Yang and Z. Wu, *Sci. Rep.*, 2015, **5**, 16628.
- 34 T. Okada, T. Kawawaki, K. Takemae, S. Tomihari, T. Kosaka, Y. Niihori and Y. Negishi, *J. Phys. Chem. Lett.*, 2024, **15**, 1539–1545.
- 35 C. Zhang, S. Takada, M. Kölzer, T. Matsumoto and K. Tatsumi, *Angew. Chem., Int. Ed.*, 2006, **45**, 3768–3772.
- 36 M. Kriege and G. Henkel, *Z. Naturforsch. B*, 1987, **42**, 1121–1128.
- 37 B.-K. Koo, E. Block, H. Kang, S. Liu and J. Zubieta, *Polyhedron*, 1988, **7**, 1397–1399.
- 38 Y. Yamashina, Y. Kataoka and Y. Ura, *Eur. J. Inorg. Chem.*, 2014, **2014**, 4073–4078.
- 39 Y. Yamashina, Y. Kataoka and Y. Ura, *Inorg. Chem.*, 2014, **53**, 3558–3567.
- 40 Y. Shichibu, K. Yoshida and K. Konishi, *Inorg. Chem.*, 2016, **55**, 9147–9149.
- 41 Y. Akanuma, T. Imaoka, H. Sato and K. Yamamoto, *Angew. Chem., Int. Ed.*, 2021, **60**, 4551–4554.
- 42 M. Zhu, S. Zhou, C. Yao, L. Liao and Z. Wu, *Nanoscale*, 2014, **6**, 14195–14199.
- 43 H. N. Kagalwala, E. Gottlieb, G. Li, T. Li, R. Jin and S. Bernhard, *Inorg. Chem.*, 2013, **52**, 9094–9101.
- 44 R. Angamuthu and E. Bouwman, *Phys. Chem. Chem. Phys.*, 2009, **11**, 5578–5583.
- 45 D. R. Kauffman, D. Alfonso, D. N. Tafen, J. Lekse, C. Wang, X. Deng, J. Lee, H. Jang, J.-s. Lee, S. Kumar and C. Matranga, *ACS Catal.*, 2016, **6**, 1225–1234.
- 46 K. S. Joya, L. Sinatra, L. G. AbdulHalim, C. P. Joshi, M. N. Hedhili, O. M. Bakr and I. Hussain, *Nanoscale*, 2016, **8**, 9695–9703.
- 47 A. Datta, N. S. John, G. U. Kulkarni and S. K. Pati, *J. Phys. Chem. A*, 2005, **109**, 11647–11649.
- 48 H. Seong, Y. Jo, V. Efremov, Y. Kim, S. Park, S. M. Han, K. Chang, J. Park, W. Choi, W. Kim, C. H. Choi, J. S. Yoo and D. Lee, *J. Am. Chem. Soc.*, 2023, **145**, 2152–2160.
- 49 A. Bondi, *J. Phys. Chem.*, 1964, **68**, 441–451.
- 50 R. D. Shannon and C. T. Prewitt, *Acta Crystallogr., Sect. B: Struct. Crystallogr. Cryst. Chem.*, 1969, **25**, 925–946.
- 51 J. Chen, L. Liu, X. Liu, L. Liao, S. Zhuang, S. Zhou, J. Yang and Z. Wu, *Chem. -Eur. J.*, 2017, **23**, 18187–18192.
- 52 S. Hossain, Y. Imai, Y. Motohashi, Z. Chen, D. Suzuki, T. Suzuki, Y. Kataoka, M. Hirata, T. Ono, W. Kurashige, T. Kawawaki, T. Yamamoto and Y. Negishi, *Mater. Horiz.*, 2020, **7**, 796–803.
- 53 X. Liu, J. Yuan, J. Chen, J. Yang and Z. Wu, *Part. Part. Syst. Character.*, 2019, **36**, 1900003.
- 54 X. Cheng, X. Sui, J. Xu, X. Liu, M. Chen and Y. Zhu, *RSC Adv.*, 2021, **11**, 32526–32532.

View Article Online

DOI: 10.1039/D4NB01457G



All data generated in this study are provided in the manuscript and Supplementary Information.

Open Access Article. Published on 06 January 2025. Downloaded on 1/15/2025 8:11:17 AM.  
This article is licensed under a Creative Commons Attribution-NonCommercial 3.0 Unported Licence.

